Eigenmode analysis of the electromagnetic field scattered by an elliptic cone

M. Kijowski and L. Klinkenbusch

Institute of Electrical and Information Engineering, Christian-Albrechts-Universität zu Kiel, Germany

Abstract. The vector spherical-multipole analysis is applied to determine the scattering of a plane electromagnetic wave by a perfectly electrically conducting (PEC) semi-infinite elliptic cone. From the eigenfunction expansion of the total field in the space outside the elliptic cone, the scattered far field is obtained as a multipole expansion of the free-space type by a single integration over the induced surface currents. As for the evaluation of the free-space-type expansion it is necessary to apply suitable series transformation techniques, a sufficient number of eigenfunctions has to be considered. The eigenvalues of the underlying two-parametric eigenvalue problem with two coupled Lamé equations belong to the Dirichlet- or the Neumann condition and can be arranged as so-called eigenvalue curves. It has been observed that the eigenvalues are in two different domains: In the first one Dirichlet- and Neumann eigenvalues are either nearly coinciding, while in the second one they are strictly separated. The eigenfunctions of the first (coinciding) type look very similar to free-space modes and do not contribute to the scattered field. This observation allows to significantly improve the determination of diffraction coefficients.

1 Introduction

Electromagnetic scattering by a PEC elliptic cone is of practical importance for several reasons. First, the geometry includes a tip, and the related tip-diffraction coefficient could be used to improve asymptotically valid methods like GTD and UTD in describing scattering by complex electrically large systems. Second, as the geometry can be treated mostly analytically using sphero-conal coordinates and the vector spherical-multipole expansion, the obtained results (e.g., for

a finite elliptic cone with the degenerations sector and circular cone) can serve as a reference for numerical computations. Scattering by circular and (less often) by elliptic cones have been treated by many authors in the literature. Summaries on the different approaches can be found in Bowman et al. (1987); Klinkenbusch (2007). This paper starts with a description of sphero-conal coordinates which are used to describe the elliptic cone geometry. For an incident plane electromagnetic wave the exact total field outside and the corresponding surface current on the elliptic cone are determined by a spherical-multipole (eigenfunction) expansion based on suitable solutions of the scalar homogeneous Helmholtz equation. The far field is then found as a free-space type spherical-multipole expansion from an integration over the surface current. In sphero-conal coordinates the solution of the scalar Helmholtz equation leads to a two-parametric eigenvalue problem with two coupled Lamé differential equations, that is, the differential equations of the periodic and of the non-periodic Lamé functions. The two separation parameters can be arranged on so-called eigenvalue curves on which the Dirichlet- and Neumann eigenvalues are discretely distributed. It turns out that the numerical determination of some of these eigenvalues is difficult, however, as will be shown exactly these eigenvalues do not significantly contribute to the scattered far field and can be automatically sorted out. Finally, this procedure leads to an improved accuracy in determining the scattering coefficient magnitudes and phases.

Fig. 1. Sphero-conal coordinate surfaces.

2 Sphero-conal coordinates

Sphero-conal coordinates r, ϑ, φ are related to Cartesian coordinates by (Boersma and Jansen, 1990)

$$
\begin{aligned}
x &= r\sin\vartheta\cos\varphi \\
y &= r\sqrt{1-k^2\cos^2\vartheta}\,\sin\varphi \\
z &= r\cos\vartheta\sqrt{1-k'^2\sin^2\varphi}
\end{aligned}
\tag{1}
$$

The ranges of the values are $0 \le r < \infty$, $0 \le \vartheta \le \pi$, $0 \le \varphi \le 2\pi$ and the ellipticity parameters k and k' satisfy

$$
0 \le k, k' \le 1; \quad k^2 + k'^2 = 1.
\tag{2}
$$

The coordinate surfaces are shown in Fig. 1. The elliptic cone is identical to the coordinate surface $\vartheta = \vartheta_0$ and can be characterized by the half opening angles $\vartheta_x = \vartheta_0$ and $\vartheta_y = \arccos(k\cos\vartheta_0)$. The normalized metric scaling coefficients are given by

$$
s_\vartheta = \frac{1}{r}\left|\frac{\partial \boldsymbol{r}}{\partial \vartheta}\right| = \sqrt{\frac{k^2\sin^2\vartheta + k'^2\cos^2\varphi}{1-k^2\cos^2\vartheta}}
\tag{3}
$$

$$
s_\varphi = \frac{1}{r}\left|\frac{\partial \boldsymbol{r}}{\partial \varphi}\right| = \sqrt{\frac{k^2\sin^2\vartheta + k'^2\cos^2\varphi}{1-k'^2\sin^2\varphi}}
\tag{4}
$$

Note that the elliptic cone includes several interesting degenerations: For $k = 1$ the elliptic cone turns into a circular cone while $\vartheta_0 = \pi$ describes a plane angular sector with half-opening angle $\arccos(k)$.

3 Eigenfunction expansion of the total field

In a linear, homogeneous, and isotropic domain outside the elliptic cone the total electromagnetic field can be derived as a multipole (eigenfunction) expansion in sphero-conal coordinates which is based on the corresponding solution of the scalar homogeneous Helmholtz equation

$$
\Delta\Psi(\boldsymbol{r}) + \kappa^2\Psi(\boldsymbol{r}) = 0
\tag{5}
$$

where $\kappa = \omega\sqrt{\mu\varepsilon}$ denotes the wave number. A first separation ansatz

$$
\Psi(r,\vartheta,\varphi) = R(r)Y(\vartheta,\varphi)
\tag{6}
$$

with a first separation constant $\nu(\nu+1)$ leads to the differential equation of the spherical Bessel functions with solutions $z_\nu(\kappa r)$ and to the eigenvalue equation of surface spherical harmonics which are referred to as Lamé products in case of sphero-conal coordinates

$$
(\boldsymbol{r}\times\nabla)^2 Y_\nu(\vartheta,\varphi) + \nu(\nu+1)Y_\nu(\vartheta,\varphi) = 0
\tag{7}
$$

For the given problem it is necessary to have solutions which are (at least) 2π – periodic in φ and fulfill canonical boundary conditions at $\vartheta = \vartheta_0$:

Dirichlet condition: $\quad Y_\sigma(\vartheta,\varphi)|_{\vartheta=\vartheta_0} = 0$
$\tag{8}$

Neumann condition: $\quad \left.\dfrac{\partial Y_\tau(\vartheta,\varphi)}{\partial \vartheta}\right|_{\vartheta=\vartheta_0} = 0$
$\tag{9}$

A second separation ansatz of the form

$$
Y_\nu(\vartheta,\varphi) = \Theta_\nu(\vartheta)\Phi_\nu(\varphi)
\tag{10}
$$

with a second separation constant λ yields two ordinary differential equations:

$$
\sqrt{1-k'^2\sin^2\varphi}\,\frac{d}{d\varphi}\left(\sqrt{1-k'^2\sin^2\varphi}\,\frac{d\Phi_\nu}{d\varphi}\right)
$$
$$
+ \left[\lambda - \nu(\nu+1)k'^2\sin^2\varphi\right]\Phi_\nu = 0
\tag{11}
$$

$$
\sqrt{1-k^2\cos^2\vartheta}\,\frac{d}{d\vartheta}\left(\sqrt{1-k^2\cos^2\vartheta}\,\frac{d\Theta_\nu}{d\vartheta}\right)
$$
$$
+ \left[\nu(\nu+1)(1-k^2\cos^2\vartheta) - \lambda\right]\Theta_\nu = 0
\tag{12}
$$

Equation (11) is referred to as the differential equation of the periodic Lamé functions $\Phi_\nu(\varphi)$ while Eq. (12) represents the differential equation of the non-periodic Lamé functions $\Theta_\nu(\vartheta)$. The periodic Lamé functions can be described as infinite Fourier series and the non-periodic Lamé functions are expanded into infinite series using associated Legendre functions of the 1st kind (Boersma and Jansen, 1990). In case of solutions in the free unbounded space the eigenvalues are integers ($\nu = n = 1,2,3,..$), the series become finite, and consequently the solutions turn into periodic and non-periodic Lamé polynomials $\Phi_{nm}(\varphi)$ and $\Theta_{nm}(\vartheta)$, respectively.

For a given value of ν and of the parameter k^2 the corresponding second separation constant λ can be numerically determined. The resulting (ν,λ)-pairs lie on characteristic eigenvalue curves sorted by numbers $m = 0,1,2,...$ Any arbitrary pair of eigenvalues (ν,λ) lying on the eigenvalue curves
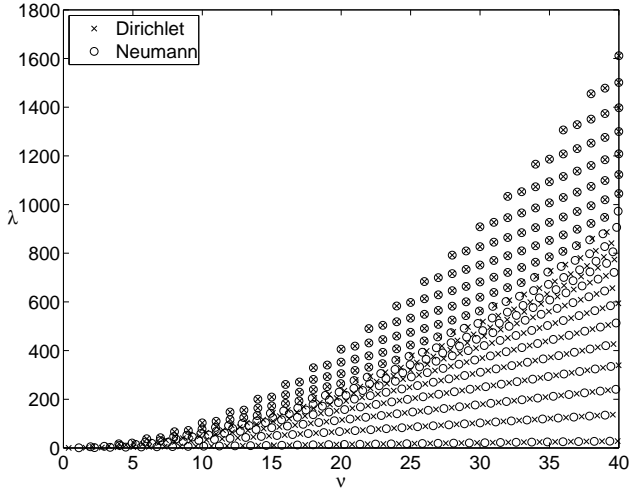
Fig. 2. Eigenvalue curves $\lambda(\nu)$ for $k^2 = 0.5$ with Dirichlet eigenvalues ($\times$) and Neumann eigenvalues ($\circ$).

leads to a valid solution of the eigenvalue equation of the Lamé products Eq. (7). Additional Dirichlet- and Neumann boundary conditions imposed upon the non-periodic Lamé functions Θ_ν at ϑ_0 result in a discrete spectrum of eigenvalue pairs (ν_i, λ_i) $(i = 1, 2, 3, ..)$ lying on the eigenvalue curves. Figure 2 exemplarily shows the eigenvalue curves with discrete Dirichlet- and Neumann eigenvalues. Due to the Sturm-Liouville properties of the Lamé differential equations the discrete Dirichlet- and Neumann eigenvalues strictly must alternate on the eigenvalue curves (Boersma and Jansen, 1990).

Outside the PEC elliptic cone the total electromagnetic field can be expressed in the form of a spherical-multipole (eigenfunction) expansion (Stratton, 1941; Blume and Klinkenbusch, 1999)

$$E^{\text{tot}}(\boldsymbol{r}) = \sum_\sigma a_\sigma \boldsymbol{N}_\sigma(\boldsymbol{r}) + \frac{Z}{j} \sum_\tau b_\tau \boldsymbol{M}_\tau(\boldsymbol{r}) \tag{13}$$

$$H^{\text{tot}}(\boldsymbol{r}) = \frac{j}{Z} \sum_\sigma a_\sigma \boldsymbol{M}_\sigma(\boldsymbol{r}) + \sum_\tau b_\tau \boldsymbol{N}_\tau(\boldsymbol{r}) \tag{14}$$

where the expansion functions which are referred to as the vector spherical-multipole functions can be derived from the elementary solutions of the scalar homogeneous Helmholtz equation $\Psi_\nu(\boldsymbol{r})$ by

$$\begin{aligned} \boldsymbol{M}_\nu(\boldsymbol{r}) &= (\boldsymbol{r} \times \nabla) \Psi_\nu(\boldsymbol{r}) \\ &= z_\nu(\kappa r) \boldsymbol{m}_\nu(\vartheta, \varphi) \end{aligned} \tag{15}$$

$$\begin{aligned} \boldsymbol{N}_\nu(\boldsymbol{r}) &= \frac{1}{\kappa} [\nabla \times (\boldsymbol{r} \times \nabla)] \Psi_\nu(\boldsymbol{r}) \\ &= -\frac{z_\nu(\kappa r)}{\kappa r} n(n+1) Y_\nu(\vartheta, \varphi) \hat{r} \\ &\quad - \frac{1}{\kappa r} \frac{d}{dr} [r z_\nu(\kappa r)] \boldsymbol{n}_\nu(\vartheta, \varphi) \end{aligned} \tag{16}$$

with $\hat{r} = \boldsymbol{r}/r$ denoting the unit vector and $\kappa = \omega \sqrt{\varepsilon_0 \mu_0}$ being the wave number in the free space. The transverse vector functions are defined as

$$\boldsymbol{m}_\nu(\vartheta, \varphi) = -\frac{1}{s_\varphi} \frac{\partial Y_\nu(\vartheta, \varphi)}{\partial \varphi} \hat{\vartheta} + \frac{1}{s_\vartheta} \frac{\partial Y_\nu(\vartheta, \varphi)}{\partial \vartheta} \hat{\varphi} \tag{17}$$

$$\boldsymbol{n}_\nu(\vartheta, \varphi) = \frac{1}{s_\vartheta} \frac{\partial Y_\nu(\vartheta, \varphi)}{\partial \varphi} \hat{\vartheta} + \frac{1}{s_\varphi} \frac{\partial Y_\nu(\vartheta, \varphi)}{\partial \vartheta} \hat{\varphi} \tag{18}$$

and the electric and magnetic multipole amplitudes are given by a_σ and b_τ, respectively. Note that the indices σ and τ symbolize the Dirichlet- and Neumann conditions as defined in Eqs. (8) and (9) to ensure the vanishing of the tangential electric field on the surface of the PEC elliptic cone. The incident plane wave is realized by locating a Hertzian dipole at infinity and multiplying the resulting field by an appropriate factor (Blume and Klinkenbusch, 1999). For a plane wave with amplitude E_0 incident from $(\theta^{\text{inc}}, \phi^{\text{inc}})$ and electrically polarized in the direction $\hat{C}$, the multipole amplitudes of the total field are found as

$$\alpha_\sigma = 4\pi E_0 \frac{e^{j(\sigma+1)\frac{\pi}{2}}}{\sigma(\sigma+1)} [\boldsymbol{n}_\sigma \cdot \hat{C}] \tag{19}$$

$$\beta_\tau = 4\pi \frac{E_0}{Z} \frac{e^{j(\tau+1)\frac{\pi}{2}}}{\tau(\tau+1)} [\boldsymbol{m}_\tau \cdot \hat{C}] \tag{20}$$

where $Z = \sqrt{\mu_0/\varepsilon_0}$ is the intrinsic impedance of the free space.

4 Spherical-multipole expansion of the scattered field

The scattered field is determined from the surface current $\boldsymbol{J}_S = -\hat{\vartheta} \times \boldsymbol{H}^{\text{tot}}\big|_{\vartheta_0}$ on the cone's surface by

$$E(\boldsymbol{r}) = \int_V \Gamma_0(\boldsymbol{r}, \boldsymbol{r}') \cdot \boldsymbol{J}_s(\boldsymbol{r}') dv' \tag{21}$$

where the dyadic Green's function of the free space in bilinear form is deduced as

$$\begin{aligned} \Gamma_0(\boldsymbol{r}, \boldsymbol{r}') &= \\ j\kappa \sum_{n,m} \frac{\boldsymbol{N}_{n,m}^{II}(\boldsymbol{r}) \boldsymbol{N}_{n,m}^{I}(\boldsymbol{r}')}{n(n+1)} &+ j\kappa \sum_{n,m} \frac{\boldsymbol{M}_{n,m}^{II}(\boldsymbol{r}) \boldsymbol{M}_{n,m}^{I}(\boldsymbol{r}')}{n(n+1)} \end{aligned} \tag{22}$$

At a time-factor $e^{j\omega t}$ the upper indices I and II stand for the use of spherical Bessel functions of the first kind ($z_n = j_n$) and of spherical Hankel functions of the second kind ($z_n = h_n^{(2)}$), respectively. It has been shown (Klinkenbusch, 2006) that the scattered electric far field can be written in form of a multipole expansion

$$\begin{aligned} E^{sc}(\boldsymbol{r}) &= \\ \frac{e^{-j\kappa r}}{\kappa r} &\left[-\sum_{n,m} a_{n,m}^{sc} j^n \boldsymbol{n}_{n,m} + \sum_{n,m} \frac{Z}{j} b_{n,m}^{sc} j^{n+1} \boldsymbol{m}_{n,m} \right] \end{aligned} \tag{23}$$
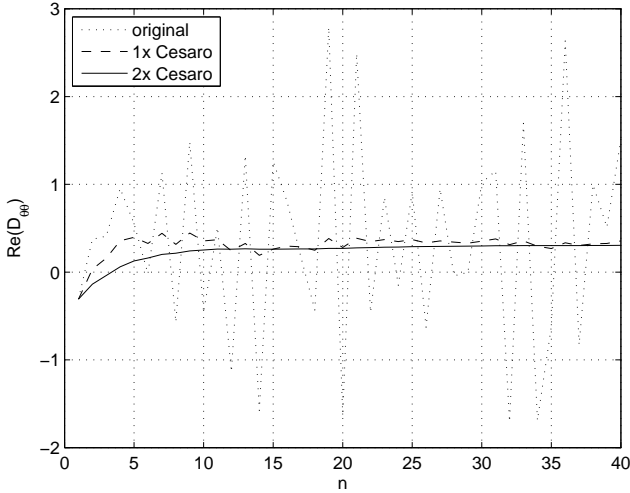
with the multipole amplitudes

Fig. 3. Partial sum sequence of the real part of the scattering coefficient $D_{\theta\theta}$ for the maximum order of $n_{\max} = 40$. Dotted curve is original partial sum sequence, dashed curve is single Cesàro transformed sequence and solid curve is double Cesàro transformed sequence.

$$a_{n,m}^{sc} = -j\Theta_{n,m}(\vartheta_0)$$

$$\left\{ \sqrt{1-k^2\cos^2\vartheta_0} \sum_\sigma \alpha_\sigma \left. \frac{d\Theta_\sigma}{d\vartheta} \right|_{\vartheta_0} \right.$$

$$\int_0^\infty \frac{j_n(\kappa r)}{r} j_\sigma(\kappa r)\kappa r dr \int_0^{2\pi} \frac{\Phi_{n,m}(\varphi)\Phi_\sigma(\varphi)}{\sqrt{1-k'^2\sin^2\varphi}} d\varphi$$

$$-\sum_\tau \frac{Z}{j}\beta_\tau \Theta_\tau(\vartheta_0)$$

$$\int_0^\infty \frac{j_n(\kappa r)}{r} \frac{[rj_\tau(\kappa r)]'}{\kappa r}\kappa r dr \int_0^{2\pi} \Phi_{n,m}(\varphi)\frac{d\Phi_\tau(\varphi)}{d\varphi} d\varphi$$

$$+\sum_\tau \frac{Z}{j}\beta_\tau \Theta_\tau(\vartheta_0)\frac{\tau(\tau+1)}{n(n+1)}$$

$$\left. \int_0^\infty \frac{[rj_n(\kappa r)]'}{\kappa r} \frac{j_\tau(\kappa r)}{r}\kappa r dr \int_0^{2\pi} \frac{d\Phi_{n,m}(\varphi)}{d\varphi}\Phi_\tau(\varphi)d\varphi \right\}$$

$$(24)$$

$$\frac{Z}{j}b_{n,m}^{sc} = j \left. \frac{d\Theta_{n,m}}{d\vartheta} \right|_{\vartheta_0} \sqrt{1-k^2\cos^2\vartheta_0} \sum_\tau \frac{Z}{j}\beta_\tau \Theta_\tau(\vartheta_0)$$

$$\frac{\tau(\tau+1)}{n(n+1)} \int_0^\infty j_n(\kappa r)\frac{j_\tau(\kappa r)}{r}\kappa r dr \int_0^{2\pi} \frac{\Phi_{n,m}(\varphi)\Phi_\tau(\varphi)}{\sqrt{1-k'^2\sin^2\varphi}} d\varphi.$$
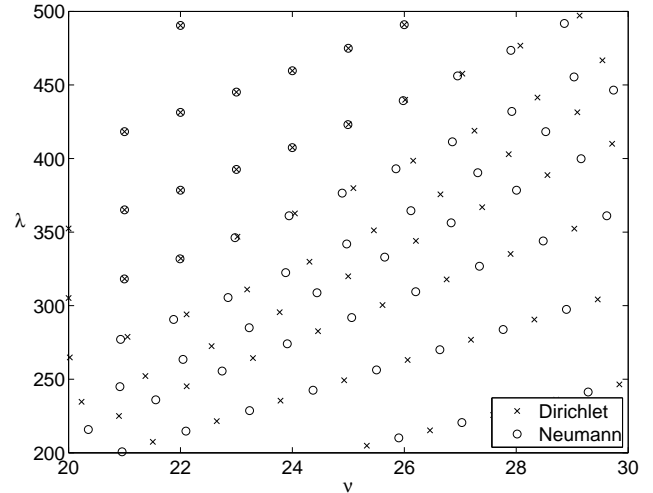
$$(25)$$

Fig. 4. Detailed view of the eigenvalue curves of Lamé functions for $k^2 = 0.5$ with Dirichlet- ($\times$) and Neumann ($\circ$) eigenvalues.

Finally, the scattered far field can be written as a function of the incident field by means of a scattering matrix as

$$\begin{pmatrix} E_\theta^{sc}(\theta,\phi) \\ E_\phi^{sc}(\theta,\phi) \end{pmatrix} = \frac{e^{-j\kappa r}}{\kappa r} \begin{pmatrix} D_{\theta\theta} & D_{\theta\phi} \\ D_{\phi\theta} & D_{\phi\phi} \end{pmatrix} \begin{pmatrix} E_\theta^{\mathrm{inc}}(\theta',\phi') \\ E_\phi^{\mathrm{inc}}(\theta',\phi') \end{pmatrix} \quad (26)$$

While the series in Eqs. (24) and (25) converge and yield stable multipole amplitudes of the scattered field, the resulting series in Eq. (23) do not converge. In order to obtain a meaningful limiting value it is necessary to apply a suitable sequence transformation. In contrast to nonlinear techniques (like the Shanks transform) linear sequence transformations always yield consistent results. For the linear Cesàro transform the transformed partial sum sequence s_n' is obtained from the original partial sum sequence s_n by

$$s_n' = \frac{s_0+s_1+s_2+...+s_n}{n+1}, \quad n=0,1,2,.. \quad (27)$$

The sequence transformation can be repeatedly applied to enforce faster convergence of the resulting partial sum sequence. Figure 3 shows the double transformed partial sum sequence of the scattering coefficent $D_{\theta\theta}$ as a function of n. Clearly, a higher order of the original series and hence a higher number of eigenvalues is desired to obtain more accurate results. In order to increase the maximum number of available eigenvalues and eigenfunctions it is necessary to investigate the relevance of eigenvalues and eigenmodes which will be sketched in the following section.

5   Eigenmode analysis

In Fig. 2 it has been shown that the discrete (ν, λ)-pairs arranged in an eigenvalue-curve scheme which can approximately be divided into an upper region where Dirichlet- and
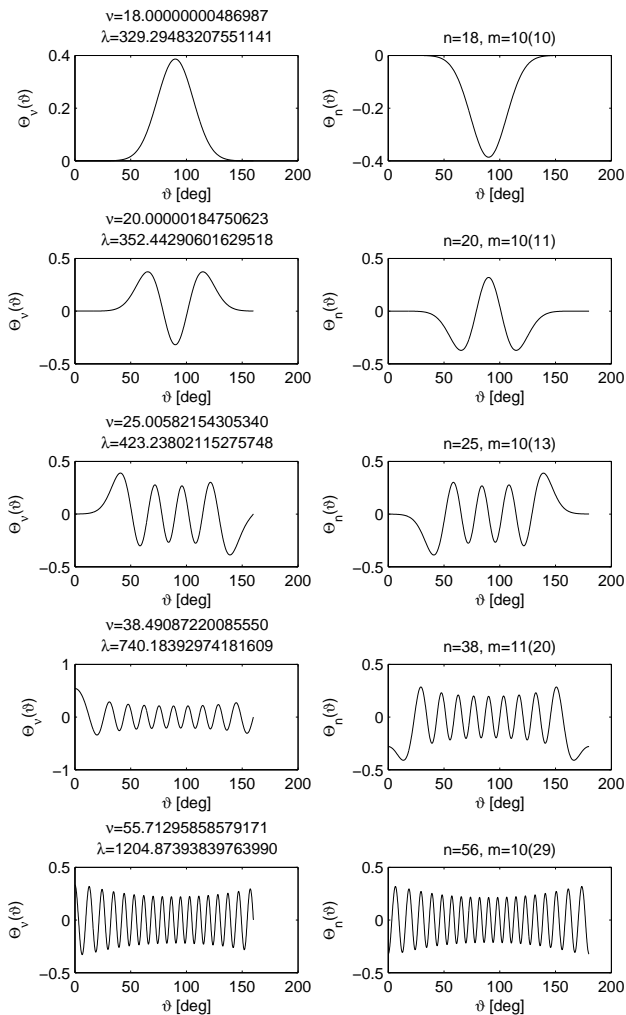
Fig. 5. Sequence of non-periodic Lamé functions $\Theta_\nu(\vartheta)$ to the Dirichlet boundary condition at $\vartheta_0 = 160°$, $k^2 = 0.5$ (left column) and (corresponding) non-periodic Lamé polynomials $\Theta_n(\vartheta)$ (right column), each as function of the arguments.

Neumann eigenvalues nearly coincide and into a lower region where Dirichlet- and Neumann eigenvalues are strictly separated. Figure 4 shows a closer view of this phenomenon revealing that the coinciding eigenvalues all are very near to integral values (integers) of ν. Since the numerical computation of these coinciding eigenvalues turns out to imply some numerical difficulties limiting the maximum number of computable eigenvalues we will now investigate that case in more detail.

The left column in Fig. 5 shows a sequence of plots of non-periodic Lamé functions each satisfying the Dirichlet boundary condition at $\vartheta_0 = 160°$ as a function of the argument ϑ. In the right column we see plots of the non-periodic Lamé polynomials (with integral eigenvalues $\nu = n$) at (n, λ)-pairs on the same eigenvalue curve nearest by those ones of the corresponding non-periodic Lamé functions.

We observe that for nearly integral eigenvalues of the non-periodic Lamé functions not only their values at ϑ_0 are vanishing but also their derivatives. Moreover, these eigenfunctions look very similar to the corresponding non-periodic Lamé polynomials. At non-integral eigenvalues only the values of the non-periodic Lamé functions vanish but not their derivatives, and their curves are different from the corresponding non-periodic Lamé polynomials, at least in the vicinity of the boundaries $\vartheta = 0$ and $\vartheta = \pi$. This general behavior is typical and can be observed for any other eigenvalue as well.

Due to numerical reasons, the computation of the nearly integral eigenvalues and -functions turns out to be difficult. However, as we can deduce from the representations of the multipole amplitudes Eqs. (24) and (25) the modes belonging to these eigenvalues do not significantly contribute to the scattered far field. Each part of Eqs. (24) and (25) has a factor of one of the following forms

$$\Theta_\tau(\vartheta_0)$$
$$\left. \frac{d\Theta_\sigma(\vartheta)}{d\vartheta} \right|_{\vartheta=\vartheta_0}$$

Clearly, if both function and derivative of a non-periodic Lamé function are small at ϑ_0, the corresponding scattering mode is also small compared to the other scattering modes. In other words, these eigenmodes of the PEC cone do not significantly lead to a surface current on the cone, or, the cone is nearly invisible for these eigenmodes. Consequently, they are very similar to free-space modes, which are characterized by integral eigenvalues.

Following this observation, these nearly-integral eigenvalues and eigenfunctions don't need to be exactly calculated, and the modified algorithm allows to calculate much more relevant eigenvalues and eigenfunctions to come to more accurate scattering coefficients.

6 Scattering coefficients

Figure 6 shows the amplitude and the phase of the electric far field scattered by a PEC semi-infinite elliptic cone illuminated by a plane wave electrically polarized in the xz plane and incident from $\theta^{\mathrm{inc}} = 105°$, $\phi^{\mathrm{inc}} = 0°$. The amplitude of the scattering coefficient $D_{\theta\theta}$ is shown for the maximum order $n_{\max} = 40$ including the integral-eigenvalue modes and $n_{\max} = 60$ excluding these non-contributing modes. The comparison between the phases shows marginal differences, however, the differences in amplitudes reveal the improvement of the results by considering more relevant eigenmodes.

Finally, Fig. 7 proves that the errors of amplitudes and phases of the scattering coefficient are actually marginal when all of the near-integer eigenvalues are neglected.
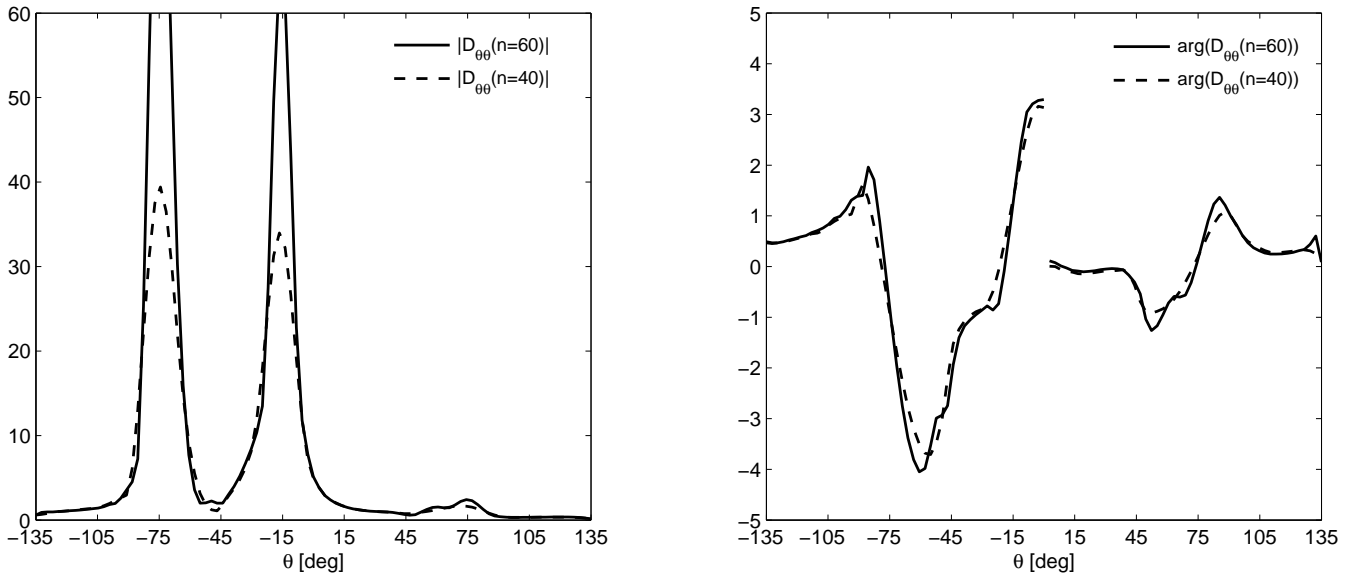
Fig. 6. Amplitude and phase of the scattering coefficient $D_{\theta\theta}$ in the xz plane of a PEC semi-infinite elliptic cone with the half opening angles $\alpha_x = 45°$, $\alpha_y = 60°$ for the order of the multipole expansion (23) $n_{max} = 40$ (dashed line) and $n_{max} = 60$ (solid line). The plane wave is incident from $\theta^{inc} = 105°$, $\phi^{inc} = 0°$.
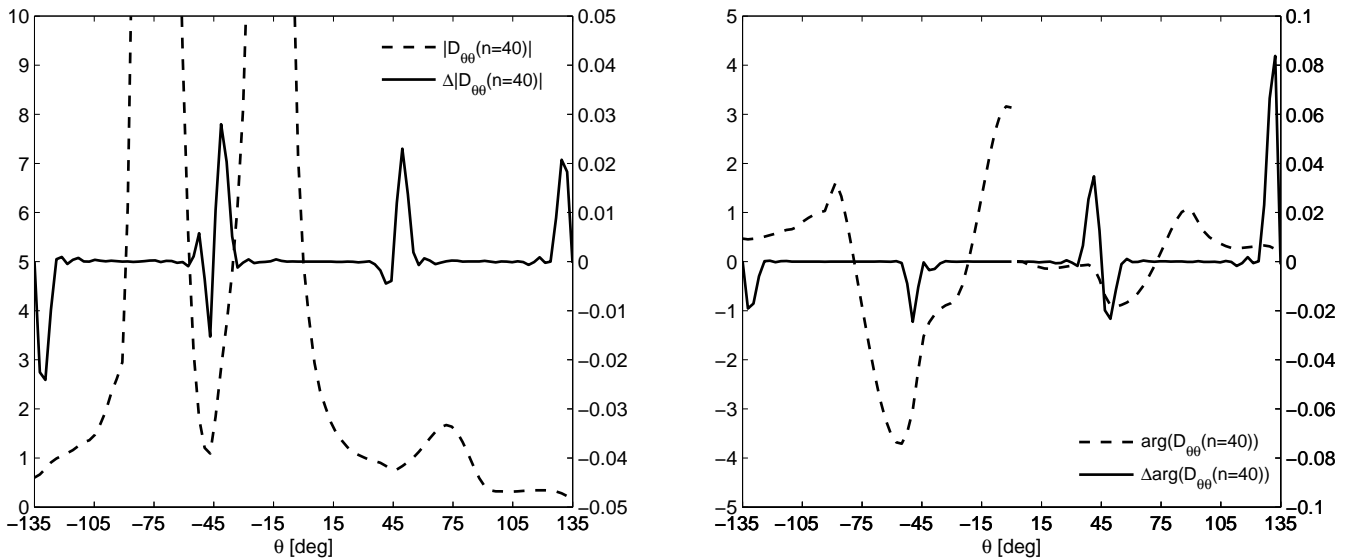
Fig. 7. Amplitude and phase of the scattering coefficient $D_{\theta\theta}$ (dashed line) in the xz plane of a PEC semi-infinite elliptic cone with the half opening angles $\alpha_x = 45°$, $\alpha_y = 60°$ and $n_{max} = 40$. The plane wave is incident from $\theta^{inc} = 105°$, $\phi^{inc} = 0°$. The solid line using the right scale is the difference between the first amplitude (phase) resulting from all eigenvalues and the second amplitude (phase) resulting from all eigenvalues except nearly integer eigenvalues.

7 Conclusions

It has been found that the accuracy of computed scattering coefficients for a PEC elliptic cone can be greatly improved if computationally difficult but non-relevant modes of the scattered field are neglected. These non-scattered modes have nearly integral eigenvalues and are very similar to the free-space modes of the incident field. Further work will include an investigation into the nature of these non-scattered modes.

References

Blume, S. and Klinkenbusch, L.: Spherical-multipole analysis in electromagnetics, in: Frontiers in Electromagnetics, edited by: Werner, D. H. and Mittra, R., 553–606, IEEE Press, New York, 1999.

Boersma, J. and Jansen, J. K. M.: Electromagnetic field singularities at the tip of an elliptic cone, EUT-Report 90-WSK-01, Faculty of Mathematics and Computing Science, Eindhoven University of Technology, Eindhoven, 1990.

Bowman, J. J., Senior, T. B. A., and Uslenghi, P. L. E.: Electromagnetic and acoustic scattering by simple shapes (Revised Printing), Hemisphere Pub. Corp., New York, 1987.

Klinkenbusch, L.: Modal Analysis of the GTD Diffraction Coefficients for the Half-Plane's Edge, Electr. Eng., 88, 337–342, 2006.

Klinkenbusch, L.: Electromagnetic scattering by semi-infinite circular and elliptic cones, Radio Sci., 42, RS6S10, doi:10.1029/2007RS003649, 2007.

Magnus, W., Oberhettinger, F., and Soni, R. P.: Formulas and theorems for the special functions of mathematical physics, Springer-Verlag, New York, 1966.

Stratton, J. A.: Electromagnetic Theory, McGraw-Hill, New York, 1941.